Journal of Environmental Chemical Engineering 12 (2024) 112990

Contents lists available at ScienceDirect

Journal of Environmental Chemical Engineering

journal homepage: www.elsevier.com/locate/jece

TiO_2 nanotubes modification by photodeposition with noble metals: Characterization, optimization, photocatalytic activity, and by-products analysis

João Lincho [a,*], Pawel Mazierski [b], Tomasz Klimczuk [c], Rui C. Martins [a], João Gomes [a], Adriana Zaleska-Medynska [b]

[a] University of Coimbra, CERES, Department of Chemical Engineering, Faculty of Sciences and Technology, Rua Sílvio Lima, Polo II, Coimbra 3030-790, Portugal
[b] Faculty of Chemistry, Department of Environmental Technology, University of Gdańsk, Gdańsk 80-308, Poland
[c] Faculty of Applied Physics and Mathematics, Gdańsk University of Technology, Gdańsk 80-233, Poland

ARTICLE INFO

Editor:

Keywords:
Noble metals
Photocatalysis
Photodeposition
TiO_2 nanotubes
Wastewater treatment

ABSTRACT

Self-organized TiO_2 nanotubes (TNTs) with 4 μm length were obtained by anodization method and calcined to obtain anatase crystallite phase. The photocatalysts were further decorated with Au, Ag, Pt or Pd nanoparticles (NPs), varying the metal loads (0.50, 0.75, 1, 2 and 5 mol%) by photodeposition. The material characterization confirmed the presence of nanoparticles in the TNTs surface, signs of the localized surface plasmon resonance (LSPR) effect for some samples and a bandgap energy of 3.1–3.2 eV. Photoluminescence measurements also confirmed that most of the samples with metallic nanoparticles had the recombination of photogenerated carriers lowered due to the trapping effect of the deposited metal NPs. The photoactivity was evaluated by phenol degradation using UV-Vis or visible radiation. Under UV-Vis, the best samples (2 and 5 mol% of Au-TNTs and 0.75, 1, and 2 mol% of Pd-TNTs) led to 97% phenol removal in 60 min while pristine TNTs reached 92% removal. Under visible radiation, the pristine and the Au-TNTs led to about 3% removal, with the best sample being 2 mol% Pd-TNTs with 14% removal in 60 min. Similar results were obtained for 1 and 5 mol% Pd-TNTs (12% and 13% of phenol removal, respectively). The by-products analysis suggest different degradation mechanisms and it is observed different kinetic rates for different metal types, metal loads or types of radiation.

1. Introduction

Titanium dioxide (TiO_2) is widely studied in different applications as photocatalytic degradation of contaminants in water or gaseous streams, hydrogen generation, energy generation and storage, gas sensing, optical devices, ceramics and in biomedicine [1,2].

Titanium is one of the most abundant metals in the world and TiO_2 presents favorable properties such as high chemical stability, non-toxicity, and low cost [3]. Most of the research involving TiO_2 is carried with powders, but this is not favorable for some applications, since it involves complex and expensive technologies to recover and reuse the material, as the case of photocatalytic oxidation of organic contaminants in water. To avoid these complications, the powder could be supported in materials (such as glass, activated carbon, silica materials, or polymeric materials) [4].

Zlamal et al., [5] obtained TiO_2 nanotubes (TNTs) by anodic oxidation and used it for the removal of the water contaminant acid orange 7, presenting better performance than supported TiO_2 P25 powder. This occurrs because the nanotubular structure presents well-defined and high surface area, better light adsorption, enhanced electron transfer, unidirectional charge transport, better structural organization, and efficient electron-hole separation [6,7]. Moreover, the TNTs obtained by anodization also present a promising solution when compared to other supported TiO_2 for the separation from liquid phase, since the nanotubes are directly formed in the Ti foil surface while other immobilization techniques require the TiO_2 production and support in another material. This implies two steps (production + supporting) while the anodization only requires one step, with the advantage of nanotubes present higher performance. Furthermore, anodization is a simple and low-cost process that requires an electrolyte solution and a simple voltage source, that also allow the TNTs scale-up [2,8].

The TiO_2 has the drawbacks of only be activated by UV radiation and

* Corresponding author.
E-mail address: jlincho@eq.uc.pt (J. Lincho).

https://doi.org/10.1016/j.jece.2024.112990
Received 16 February 2024; Received in revised form 19 April 2024; Accepted 3 May 2024
Available online 7 May 2024

the existence of photogenerated electron-hole recombination, due to its high bandgap energy (3.0–3.2 eV) [9]. These disadvantages may restrict its applications and lead to undesired costs, but both drawbacks can be reduced by modifying the TNTs. Different strategies are considered for modification, such as the doping method (of metals and non-metals), heterojunction with narrower band-gap semiconductors (such as the WO_3) or the metals decoration at the photocatalyst surface [9–11].

The surface decoration using metal nanoparticles (NPs) by photodeposition can present advantages since it uses safe chemicals and is a simple method. Noble metals are known to enhance the photocatalytic efficiency since they can act as electron traps encouraging interfacial charge movement, but it also enhances the separation of electron-holes, delaying their recombination [9,12–14]. The decoration with noble metals can also promote the formation of a Schottky barrier, which occurs due to the direct contact between the metal and the substrate, resulting in better charge separation and transfer rate [15]. Also, the presence of noble metals can promote the localized surface plasmon resonance (LSPR) effect due to its strong plasmonic effects with bands localized in the visible region, which endorses the visible light activity [9,13,15,16]. The free electrons present in the metal can oscillate collectively when irradiated by light [13,16] and the LSPR effect occurs when this oscillation is in resonance with the incident light for a determined excitation frequency, causing a strong oscillation of the electrons surface, and therefore, the visible light activity [13,16]. In an "easier" description, when visible light is irradiated to a decorated semiconductor with LSPR properties, the metal absorbs the photons and in turn injects electrons directly in the semiconductor conduction band, being then available to react [13,14,16].

Gold (Au) metallic nanoparticles can increase the photoelectron transference rate and decrease the electron-holes recombination increasing the quantum yield [12]. Similarly, silver (Ag) is also reported as an electron trapper capable of decreasing the generated pairs recombination, also promoting microorganism's deactivation [17,18]. Platinum (Pt) is a noble metal with the capacity to form the highest Schottky barrier, enhancing the photocatalytic performance due to an efficient electron-hole pairs separation and longer separation lifetime [14]. Palladium (Pd) allows a decrease in the photocatalyst inactivation, increasing its performance and promoting the scavenging of photogenerated electrons by oxygen [12]. It also presents higher chemical stability than Ag promoting better resistance to corrosion and poisoning, as well as higher thermal resistance than Au [11]. Thus, it is expected that the modification of TNTs using noble metals promotes a higher photocatalytic efficiency due to a better electron-hole pairs separation as well as activity in the visible region due to the LSPR effect.

Gross et al., [18] obtained TNTs by anodization and modified them with Ag particles using $AgNO_3$ solutions with different concentrations (0.1, 1, 10 and 100 mM) but the samples were not tested for wastewater treatment. Similarly, Lv et al., [14] modified the TNTs by photodeposition with different concentrations of an H_2PtCl_6 solution (1, 2, 3 and 4 mM) testing the samples for the photocatalytic degradation of a methyl orange solution. Unfortunately, during the research it was noted in the literature lack of works comparing TNTs modified with different metals regarding wastewater treatment purposes. Moreover, there is also a low number of works involving the optimization of decorated metal load, and when this approach is considered, the optimization considers different concentrations of metal precursor instead of considering the true metal amount.

Due to this, it is noted an opportunity to modify TiO_2 nanotubes by depositing metals considering their true concentration and comparing the metal load effect for different metals as well as the performance of modified TNTs for wastewater treatment by photocatalysis under UV-Vis and visible light. In our initial work, Lincho et al., [19] tested the effect of a low amount of Au, Pt or Pd (0.25 mol%) NPs in TNTs for the degradation of a mixture of parabens by photocatalysis (with UV and solar radiation), catalytic and photocatalytic ozonation. One conclusion of the work is that the metal amount should be investigated and optimized.

Therefore, in this work it is studied the optimization of metal decorated TNTs to enhance the photoactivity under visible radiation. The TNTs performance was evaluated considering the photocatalytic oxidation of phenol under UV-Vis and visible radiation, also considering a by-product analysis. To the best of our knowledge, this kind of strategy for the TNTs performance optimization involving four different noble metals (Au, Ag, Pt or Pd) and different metal amounts (0.5, 0.75, 1, 2 or 5 mol%) is the first to be reported.

2. Materials and methodologies

2.1. Reagents

The titanium foils (99.7%, 152 mm × 152 mm × 0.127 mm) were obtained from Sigma-Aldrich (Germany). Ammonium fluoride (NH_4F, > 96%) and phenol (> 99%) were acquired from Chempur and ethylene glycol (EG, 99%), acetone, isopropanol, and methanol were purchased from Stanlab (Poland). Resorcinol (> 99%), hydroquinone (> 99%), p-benzoquinone (> 98%) and 1,2 – dihydroxybenzene (catechol) (> 99%) were obtained from Sigma-Aldrich.

2.2. Synthesis of TiO_2 nanotubes

TiO_2 nanotubes were synthesized via one-step anodic oxidation. Firstly, the acquired Ti foil was cut to the pretended dimensions (30 mm × 50 mm × 0.127 mm) that was posteriorly cleaned in ultrasounds for 10 min, with different solvents at each time (acetone, isopropanol, methanol, and deionized water). After this, the plates were dried in a nitrogen stream.

Anodization occurred using an electrolyte solution with 0.09 M NH_4F, 98 vol% EG and 2 vol% H_2O. A voltage of 30 V was applied during 1 h between the Ti plate and a platinum mesh, both immersed in the electrolyte solution, causing the TiO_2 nanotubes to grow. After the anodization, the plates were rinsed in water and kept in the dark during 24 h. Next, the TNTs were cleaned in ultrasounds with acetone for 5 min and dried in an oven at 60 ºC for 12 h. To obtain crystalline TiO_2 nanotubes, the samples were posteriorly calcined in an oven with an air environment, for 1 h at 450 ºC (2 ºC/min), to ensure the formation of the anatase crystallite phase. This procedure is based on the previous work of Nischk et al., [20] that did an optimization of the parameters to obtain the TNTs for gas phase treatment, showing that the use of the mentioned electrolyte solution in anodization at 30 V during 1 h and the application of the above calcination parameters led to the best active and stable titanium dioxide nanotubes.

The TNTs modification occurred by photodeposition method. Different noble metal precursors were used ($HAuCl_4$, $AgNO_3$, K_2Cl_6Pt, and K_2PdCl_4) to modify the TNTs with Au, Ag, Pt and Pd, respectively. In this process, the samples (adjusted to 30 mm × 36 mm) were immersed in a defined solution composed of precursor solution and 30 mL of ethanol that acted as hole scavenger. First, to remove all the oxygen, nitrogen was bubbled to the solution for 1 h, and after, the gas stream was stopped, and the modification reactor was irradiated for 1 h by a Xe lamp (1000 W, Oriel 66021) to allow the metallic nanoparticles to be deposited in the photocatalyst's surface. Different amounts (0.50, 0.75, 1, 2 and 5 mol%) of each metal were investigated in the modification procedure.

2.3. Photocatalytic activity evaluation

The photocatalytic activity was evaluated by photodegradation of a phenol solution. For this, 8 mL of a phenol solution (20 mg/L) was placed inside a quartz reactor with the desired TNTs sample (30 mm × 18 mm × 0.127 mm), and it stayed 30 min bubbling with oxygen stream (10–12 L/h) and stirring at 500 rpm, to evaluate the adsorption capacity. Afterward, a UV-Vis Xenon lamp (1000 W, Oriel 66021, Oriel

Instruments) was used to irradiate the reactor, starting the photocatalytic reaction (60 min). Samples of 0.5 mL were taken at each 20 min. During the experiment, the reactor had the temperature controlled by a thermostatic bath at 10 ºC. For the experiments using visible wavelength, a filter (GG420) was used to cut-off the radiation below 420 nm, which was placed near the reactor. For the reuse evaluation experiments, UV-Vis radiation was considered and the same experimental protocol was carried. After each phenol photodegradation experiment, the TNTs sample was rinsed with distilled water and left to dry in dark conditions before reutilization.

2.4. Analytical procedures and materials characterization

The materials morphology was analyzed by scanning electron microscopy (SEM) analysis (JEOL JSM-7610 F). Regarding the crystallinity structure of materials, it was examined by RAMAN (Thermo Scientific DXR2 SmartRaman) equipped with DXR 532 nm laser and XRD (Phillips Xpert PROMDP) with copper Kα radiation (λ = 1.5404 Å). UV-Vis diffuse reflectance spectra (UV-Vis DRS, Shimadzu UV 2600) homed with an integrating sphere was used to analyze the material's radiation absorbance (using barium sulfate as reference for the baseline). Photoluminescent (PL) spectra analysis was conducted at room temperature using an LS-50B luminescence spectrometer equipped with a Xenon lamp and an R928 photomultiplier, emitting excitation radiation of 390 nm to the direct surface of samples at an angle of 90º. Phenol and by-product concentration were followed by HPLC-DAD (Shimadzu) with mobile phases composed of 10%:90% of acetonitrile and acidified water at 0.55 mL/min. A silichrom C18 column was used at constant temperature (40 ºC). Phenol, resorcinol, hydroquinone and 1,2 - dihydroxybenzene were detected at 225 nm while p-benzoquinone was detected at 254 nm.

3. Results and discussion

3.1. Nanotubes characterization

The sample morphology was analyzed by SEM analysis confirming the nanotubular structure (Fig. 1). The nanotubes were highly ordered and uniform, which is a characteristic of this sort of electrolyte and anodized nanotubes [21,22]. The nanotubes presented a length of 4.0 ± 0.2 μm, an internal diameter of 61.4 ± 0.2 nm and a wall thickness of 19.3 ± 4.5 nm.

The nanotubes top are opened and present some hydrous titanium oxide impurities (see Figure S1-S5) [23]. The side of the nanotube present "ripples" (also called "ribs"), and this is sporadically observed in nanotubes obtained from electrolytes with a water content higher than 2.5 vol%, being more usual for electrolytes with a water content of 5 vol % or higher [24,25].

The modified TNTs presented similar morphology and dimensions since the modification by photodeposition did not influence the morphology of the nanotubes. The samples showed the presence of metallic nanoparticles with different shapes and sizes, as shown in Fig. 2, and in Figures S1-S5. The metallic particles and/or regions with metals attached to the nanotube's mouth are highlighted and are generally clearer in SEM images.

In Fig. 2, it is possible to see the 2 mol% amount of deposited metallic nanoparticles. As the metal load increases, the nanoparticle's shape can suffer changes turning bigger and round (for Au and Ag - see Figure S1 and S2) or forming an agglomeration of the nanoparticles near the tube mouth (for Pt and Pd - see Figure S4 and S5) [26]. Also, the shape of the nanoparticles is dependent on the type of metal to be deposited (e. g. Au, Ag and Pt), this means that the shape of Au NPs deposited in nanotubes is different from the shape of deposited Ag or Pt [27]. Analyzing Fig. 2 and comparing with other works from literature, similar SEM images were obtained by Lv et al., [14] for the case of TNTs modified with different amounts of Pt, Gross et al., [18] for Ag-TNTs or Xiao [27] for the case of deposition of Au, Ag or Pt nanoparticles in TNTs.

In fact, the use of too low amount of metal can make the visualization of metallic nanoparticles easier to analyze by transmission electron microscopy (TEM) [26]. In this case, for the lowest load of nanoparticles (0.5 mol%), it is not easy to clearly see the nanoparticles by SEM but as the load increases, the visual detection becomes easier. Technologies such as the atomic layer deposition allow to deposit the nanoparticles inside and outside the nanotube's walls and in the deepest parts of the nanotubes [26,28] but to the best of our knowledge, no similar conclusion was taken with TNTs modified via photodeposition. Interestingly, Figure S3 shows the existence of metallic nanoparticles attached to the nanotube side externally.

The catalytic activity is affected by the load, chemical, and physical properties of the photoactive junction so the deposition process is crucial to enhance this activity [11]. The uniform distribution and high density of active sites across the photocatalyst surface are crucial to improve the catalytic performance [11]. Unfortunately, according to the SEM images, there is no uniform distribution of the metallic NPs over the TNTs surface, which can be a limitation of the photodeposition method. Moreover, the particle size may also influence the metal effect, and as the metal load increases the nanoparticle size also increases [11,26,28,29]. In fact, the use of a higher amount of metals does not necessarily means more active samples [26,29] since as the metal load increases, the pore aperture can decrease and the access to the TiO_2 nanotubes can be blocked, which can be responsible for activity loss [11,30]. Analyzing Figures S1 to S5, it is possible to see the agglomeration of particles and a

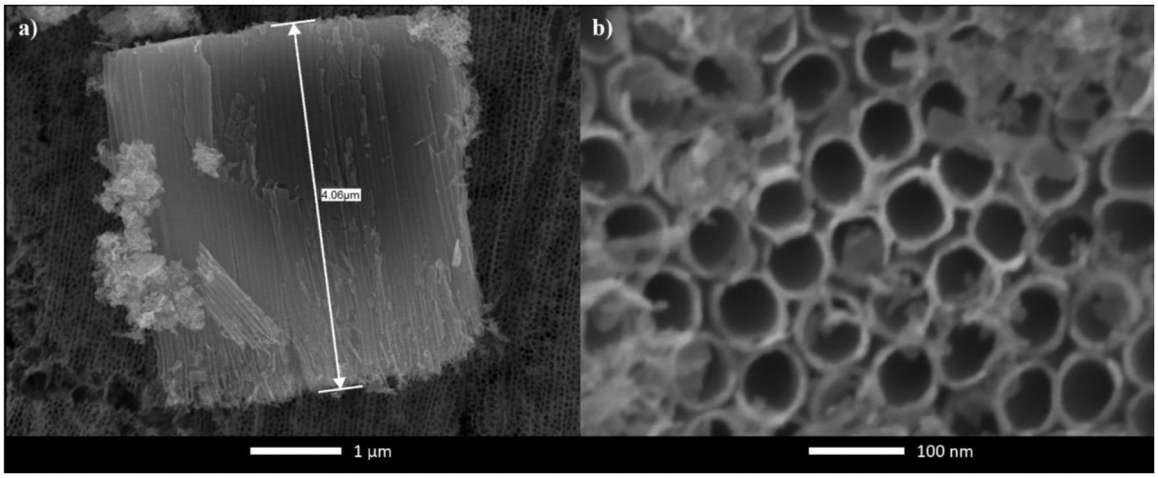

Fig. 1. SEM images of Pristine TNTs a) cross sectional view; b) surface morphology.

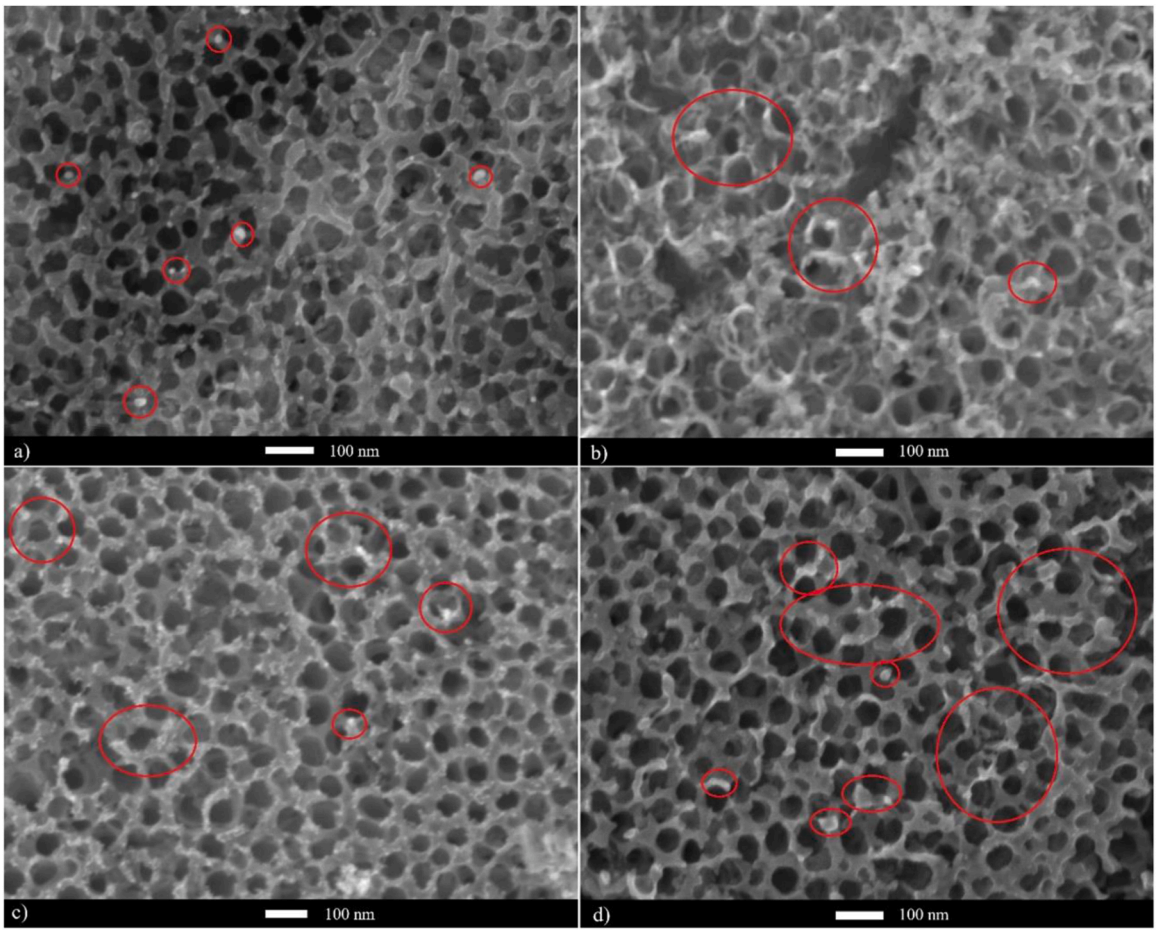

Fig. 2. SEM images of modified TNTs with: (a) 2 mol% Au; (b) 2 mol% Ag; (c) 2 mol% Pt; and (d) 2 mol% Pd.

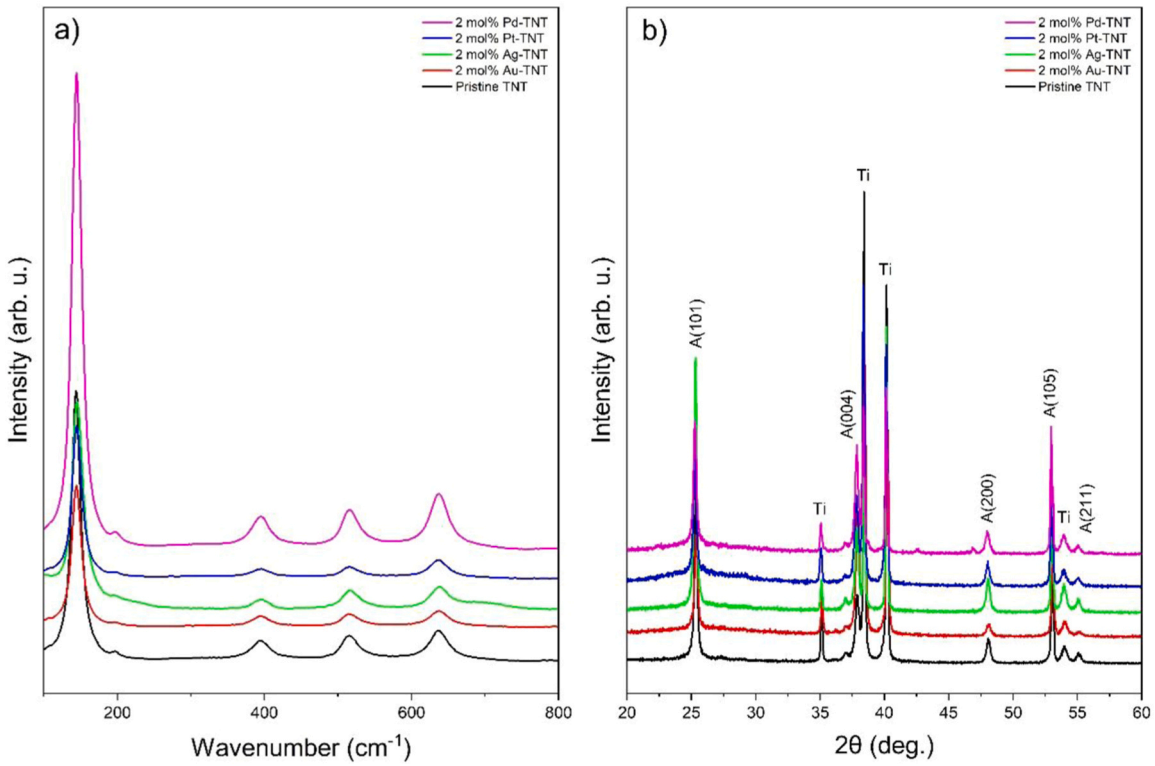

Fig. 3. Raman spectra (a) and XRD (b) of pristine and 2 mol% modified TNTs.

partial coating being formed in the tube mouth, depending on the metal used.

The metallic nanoparticles can benefit the photocatalytic system by decreasing the electron-hole recombination rate, improving the catalytic surface, or transferring electrons to the semiconductor conduction band. However, the excessive loading of metal can be prejudicial and have the opposite effect. Due to these reasons, the optimization of the metal load as well as the metal distribution over the TNTs are critical steps to obtain the best (photo)catalytic activity.

The annealing treatment was carried to convert the amorphous TiO_2 into anatase TiO_2. The crystallite structure depends on the annealing conditions and affects the photocatalyst activity [1,20,31]. The anatase crystallite phase is the best option for this case, since it allows to have a higher lifetime of the photogenerated carriers and a lower recombination rate, also with the ability of a higher light absorption capacity when compared to the other crystallite forms [32]. Moreover, in the case of a nanotubular structure, the temperature is also important to avoid any defects or collapse of the nanotubes. It was shown that an annealing temperature of 550–580 ºC causes small protrusions in the nanotubes, and their destruction is more evident as the temperature increases [31]. Therefore, temperatures up to 550 ºC can be considered without forming defects in the nanotubes, with a single anatase or a mixture of anatase and rutile phase being present in the samples [31].

In the present work, the selected temperature was 450 ºC to obtain the anatase crystallite phase, as confirmed by Raman spectroscopy with the characteristic signals at 144, 196, 391, 514 and 634 cm^{-1} [33] and by XRD with the diffraction patterns at 2θ angles of 25.32, 37.77, 47.97, 52.94, and 55.03 degrees (Fig. 3). The peaks at 2θ angles of 35.05º, 38.42º, 40.17º, and 53.84º are indicative of the hexagonal phase of the titanium metal substrate (Fig. 3b). Figures S6 and S7 present the Raman and XRD analysis for the different modified TNTs, respectively.

The radiation absorption capacity was evaluated by UV-Vis DRS spectra and the material's bandgap energy was calculated by Tauc plot methodology. Samples showed a band-gap energy of 3.1–3.2 eV, which is expected since the noble metal deposition should have small or no influence on the semiconductor bandgap energy [11,34]. The DRS spectra are presented in Fig. 4. Figures S8 and S9 compare the DRS spectra of pristine and modified samples by amount of metal and by metal.

All the samples showed a signal of absorption in the UV region due to the charge transfer from the valence band O 2p orbital to the conduction band of the Ti 3d orbital [35] while the broad absorption in the visible region (with an edge at 540 nm) is a signal of sub-bandgap states

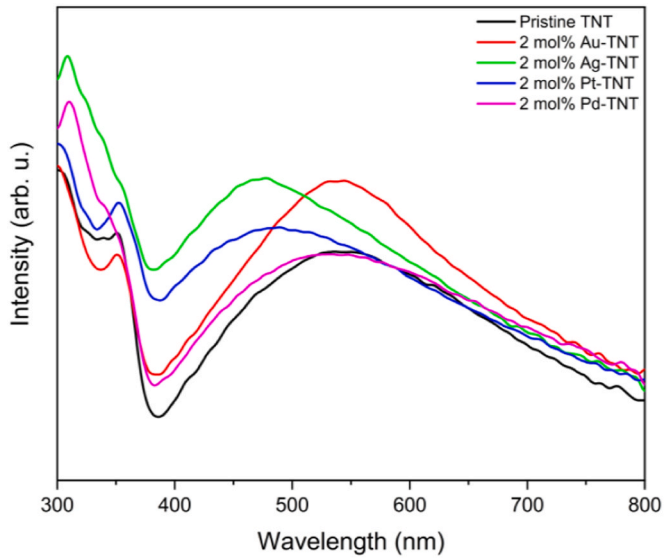

Fig. 4. UV-Vis DRS spectra of pristine TNTs and 2 mol% modified samples.

characteristic of TiO_2 nanotubular morphology [36,37]. In Fig. 4, the analysis for the 2 mol% modified TNTs shows that all the samples present better absorption than the pristine TNTs (reference sample).

The LSPR phenomenon induces unique optical properties of the metallic NPs that are dependent on its shape, size, and refractive index [38,39]. Therefore, the UV-Vis DRS spectrum and signs of the LSPR effect are dependent on these properties. The samples present different particle shapes and sizes which can justify the different UV-Vis spectrum from Fig. 4. Lal et al., [38] report a plasmon resonance frequency for Ag nanospheres of 400–550 nm, while Jeon et al., [39] reported a frequency of 500–600 nm for Au nanospheres, which seems to be concordant to what is observed if considered the SEM images of Au and Ag modified TNTs (Fig. 2) and the UV-Vis DRS spectra (Fig. 4).

The higher absorption in the DRS should be a sign of higher photoactivity, but this will be discussed in detail in Section 3.2. Moreover, the samples Ag- and Pt-TNTs show evidence of a shift to the left which is a common indicator of the LSPR effect. When this analysis is carried out by metal (Figure S8), for the Au-TNTs only the 0.5 and 0.75 mol% samples present better absorption (total or partially) in the UV region. For the visible region, only the 0.75, 2, and 5 mol% amount presents higher absorption than pristine, and the 0.75 mol% is a little shifted to the left when compared to pristine. Regarding the Ag-TNT samples, all of them present better behavior from 365 nm to the visible region with left shift signals when compared to pristine TNT. Only the 2 mol% presents better absorption in all the total UV regions, with all the other Ag-TNT samples presenting higher absorption except in a small part near the 340 nm.

In the case of Pt-TNTs, left shifts are also present. The 2 and 5 mol% amounts present higher absorption. The 0.5 and 0.75 mol% have generally equal or higher absorption, except from around 320–360 nm, in which the pristine presents higher absorbance. For the Pd-TNTs, the absorbance spectra are the most similar among the samples, and all the spectra show similar or higher absorbance (up to 425–480 nm) when compared to pristine TNT (except a case from 325 to 360 nm for the 1 mol% Pd-TNT). When this analysis is carried by amount of deposited metal (Figure S9), the 2 and 5 mol% seems to have the highest absorption when compared to the pristine TNTs, with left shifts being seen in all the used metal loads. For the 0.5 and 0.75 mol% (Figure S8), there are higher absorbances in some parts of the visible region, but these materials show in the UV region similar absorbances to pristine. Moreover, it is possible to see that these shifts are dependent on the metal and on the used amount (see in Figures S8 and S9 the case of Au and Pd, as examples).

Photoluminescence (PL) emission spectra are useful to reveal the migration, transfer, separation, and recombination processes of the photogenerated charge carriers for the different samples decorated with different metals and loads. Fig. 5 presents the PL analysis for the selected samples, while Figures S10 and S11 present the measurements for all synthetized samples.

The PL is generated due to the recombination of photoexcited carriers, and generally, a high PL intensity is related to a higher recombination rate of the photogenerated carriers and vice versa [40,41], in which a lower intensity should benefit the photocatalytic processes. The metals can act as electron trappers and inhibit the recombination of the photogenerated carriers [17], which should decrease the PL intensity. In general, for almost all the analyzed samples (see Fig. 5 and Figures S10 and S11), the metallic NPs promote a reduction of the PL intensity which should be evidence of a lower recombination rate. Also, as presented in Fig. 5, it is possible to identify emissions peaks at 421, 449, 484 and 530 nm, being a characteristic of this nanotubular material [42]. The peak 421 nm is related to the charge transference from Ti^{3+} to O^{2-} in the octahedron $[TiO_6]^{8-}$, the 449 and 484 nm peaks are related to surface and structural defects, and the peak 530 nm is pointed out to the radiative recombination of charge carriers [42–44].

For the 2 mol% samples, the Au is the sample that shows lower recombination followed by Pt and Ag. The 2 mol% Pd-TNTs present

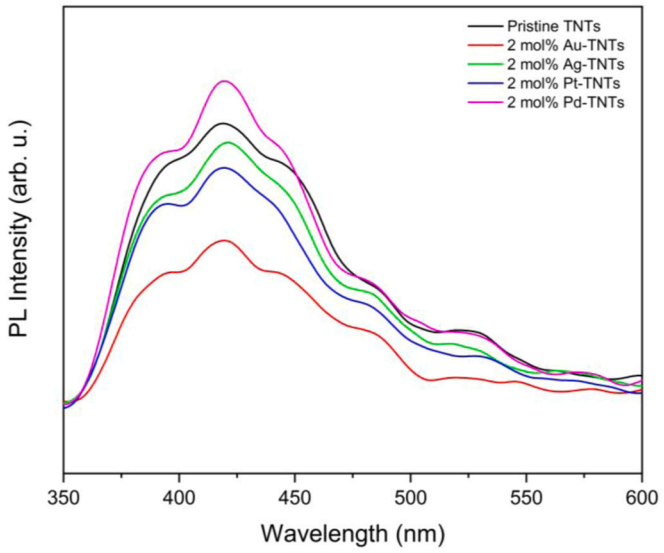

Fig. 5. PL measurements of pristine TNTs and 2 mol% modified samples.

higher intensity than the pristine sample. Considering different metals (Figure S10), the samples modified with Pd present similar profiles as the pristine sample, while with the other metals present the materials show, in general, lower recombination rates. Moreover, gold modified samples are always the samples with lower intensity, with an expressive decrease compared to the reference sample, with the Pt-TNTs also showing a lower intensity. By analyzing the PL measurements by the amount of deposited metal (Figure S11), Au-TNTs present the lowest peak intensity with similar profiles, while the Pd-TNTs present similar profiles compared to the pristine TNTs. Ag- and Pt-TNTs present different profiles depending on the metal load.

3.2. Photocatalytic activity – Phenol degradation with UV-Vis and Vis radiation

Phenol abatement was chosen for the photocatalytic activity evaluation since phenol is commonly present in industrial wastewater and it has potential adverse effects on ecosystems and humans [45]. When compared to other types of electrolytes, organic electrolytes lead to TNTs with high activity and improved properties such as crystal structure stability [46,47] which also motivate the use of this kind of electrolyte for the TNTs synthesis.

Previous experiments showed that the photolysis of phenol led to 3% and 1% removal in 60 min, for UV-Vis and Vis radiation, respectively [6]. Therefore, the degradation of phenol occurred due to the formation and interaction of oxidizing species. The comparison of the phenol degradation after 60 min irradiation for the different modified samples under UV-Vis and visible radiation is presented in Fig. 6.

The photocatalytic oxidation of phenol using UV-Vis radiation led to almost complete degradation in 60 min for all the samples, with pristine TNTs leading to 92% removal. The best results were obtained with 2 and 5 mol% Au-TNTs and with 0.75, 1 and 2 mol% Pd-TNTs (see Fig. 6, and Figure S16).

From Fig. 6, an interesting result is possible to obtain for the 0.5 mol % samples, in which all of them showed worse behavior than the pristine TNTs. For some reason, this low amount of metal seems to present a negative effect and cause a lower phenol degradation, but, when the metal amount is increased (with each metal presenting different behavior) it is possible to obtain better performances, which suggests the possibility and benefit of optimizing the metal load deposition.

In the case of Au, the increase in the metal load led to an increase in the phenol photodegradation, with the 2 mol% and 5 mol% having the same behavior, which suggests the 2 mol% is best loading amount. For Ag-TNTs, all the samples were worse than pristine which should be related to a negative effect under UV-Vis radiation (probably due to a higher capture of electrons by silver), although the influence of metal load can be visualized among the silver samples. In the case of Pt, the

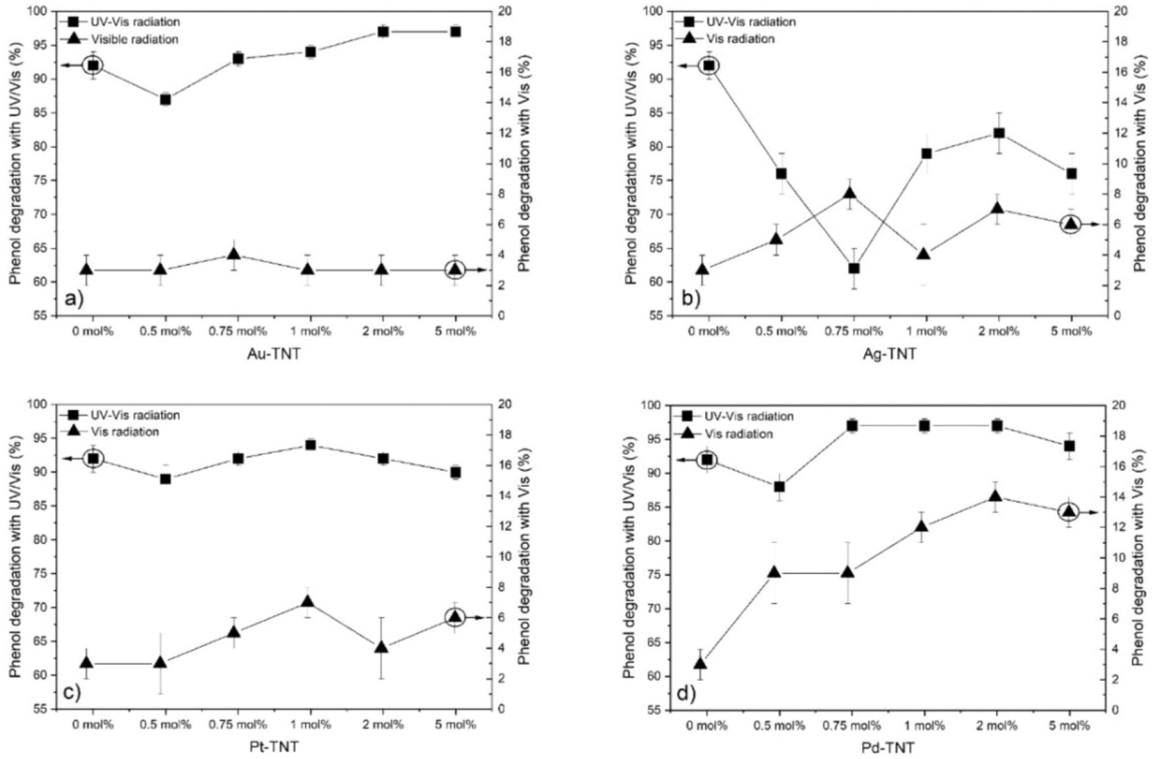

Fig. 6. Phenol photodegradation with Pristine and modified TNTs for UV-Vis and Vis radiation: (a) Au-TNTs; (b) Ag-TNTs; (c) Pt-TNTs and (d) Pd-TNTs.

increase in the metal load leads to the best degradation value for 1 mol% load, but the differences among the several loads are not so high. This can be related to a good dispersion of platinum over the nanotube's mouth when compared to the other metals (see Fig. 2 and Figure S4). For the case of Pd-TNTs, the 0.75, 1 and 2 mol% present similar results, which suggests a maximum performance. However, increasing to 5 mol % causes a decrease in the phenol degradation which can be related to excessive amount of NPs that may block the nanotubes surface and active sites [30]. The metal load also affects the nanoparticle's size, which in turn may influence the catalytic activity [11,26,28,29]. As an example for water decontamination, Merenda et al., [11] reported a particle size of 5.1 nm as the best Pd particle dimension, when compared to sizes of 7.6 or 13.6 nm, for two different types of radiation. From this study, it is possible to understand that the highest amount of metal does not conduct to the best active sample, which can be related to the nanoparticle size. Also in this case, the best average size was the same for both radiations under test, but for other cases, different conclusions can be taken [26,29]. Concluding, the metal load influences the nanoparticle's size which affects the photocatalytic activity, and therefore, the use of decorated TNTs should be optimized to maximize its performance, and different apparatus (radiation, decorated metal, etc.) can lead to different conclusions.

Table 1 presents the degradation and the kinetic constants for the phenol abatement assuming a pseudo-first order rate.

The samples with 2 and 5 mol% Au-TNTs and 2 mol% Pd-TNTs increased the reaction kinetics from 0.044 to about 0.060 min^{-1}, while the samples 0.75 and 1 mol% Pd-TNTs increased to about 0.055 min^{-1}, which represent an enhance in the degradation rate by almost 34% and 25% respectively, when compared to pristine TNTs. Among the platinum samples, only the 1 mol% Pt-TNTs presented higher kinetics than the pristine, with the other amounts presenting worse results. Also, due to the low phenol degradation, the samples modified with Ag presented the worst degradation kinetics obtained, with the best Ag sample (2 mol% Ag-TNTs) presenting a degradation rate of 0.0278 min^{-1} which is worse about 35% than the bare TNTs.

With this, it seems that for this type of radiation the Ag and Pt metals are not capable of increasing the phenol degradation rate when compared to the pristine TNTs. Therefore, other analyses (such as mineralization, by-product formation or toxicity studies) or use in other AOPs (such as ozonation) should be carried out to understand if the materials can be advantageous to the contaminant's degradation. It is known that silver may present a good effect in the deactivation of microorganisms, which can be an important consideration for the presence of this metal in the reactional medium of real wastewater.

Table 1
Photocatalytic activity of materials.

Photocatalyst		Kinetic constant rates (min^{-1})	
		UV-Vis	Vis
Pristine TNTs		0.0440	0.0001
Au-TNTs	0.50 mol%	0.0335	**0.0003**
	0.75 mol%	0.0432	0.0001
	1 mol%	**0.0460**	**0.0003**
	2 mol%	**0.0602**	**0.0002**
	5 mol%	**0.0600**	0.0001
Ag-TNTs	0.50 mol%	0.0218	**0.0003**
	0.75 mol%	0.0154	**0.0006**
	1 mol%	0.0253	**0.0003**
	2 mol%	0.0278	**0.0006**
	5 mol%	0.0228	**0.0002**
Pt-TNTs	0.50 mol%	0.0347	**0.0005**
	0.75 mol%	0.0417	**0.0007**
	1 mol%	**0.0464**	**0.0005**
	2 mol%	0.0414	**0.0005**
	5 mol%	0.0381	**0.0005**
Pd-TNTs	0.50 mol%	0.0346	**0.0009**
	0.75 mol%	**0.0559**	**0.0011**
	1 mol%	**0.0544**	**0.0015**
	2 mol%	**0.0608**	**0.0015**
	5 mol%	**0.0452**	**0.0014**

*In bold are the results better than those obtained with pristine TNTs

For Vis radiation, the results indicate that in general, the use of Ag, Pt and Pd benefited from the LSPR effect, while the ~3% degradation obtained with the Au samples could be related to an adsorption phenomenon. However, the 2 mol% Au-TNTs and the pristine TNTs led to the formation of benzoquinone, which suggests the decomposition of phenol by oxidizing radicals (this will be discussed in detail in Section 3.3.2). The highest performances under this type of radiation were obtained by Pd with the 1, 2, and 5 mol% loads obtaining the same phenol degradation in 60 min, respectively (Table 1 and Fig. 6). The kinetics considering the Vis radiation are much slower than when compared to UV-Vis radiation. The highest kinetic rate was achieved for the 1 mol% and 2 mol% Pd-TNTs with 0.015 min^{-1} compared to the pristine TNTs that showed a 0.001 min^{-1} degradation rate. In general, all the samples presented higher degradation rate, presenting the benefit of having the metal presence. Even for the Ag and the Pt metals, the kinetics were higher about 2 and 7 times, and this increase is related to the LSPR effect. For visible radiation, Ag and Pt seems to present benefits, although the highest increase in the degradation performance be obtained with Pd.

Considering the selected samples (2 mol%), Fig. 7 presents the degradation profiles for UV-Vis and Vis radiation. Figure S12-S17 provides additional information about phenol degradation. The experiments were made in duplicate, and the error does not exceed 3%.

Analyzing the degradation profiles, it is possible to see that the degradation results do not present the behavior that would be expected considering the material's DRS spectra (Fig. 4). For example, the Ag-TNTs should present better activity in the UV region due to the higher absorbance detected in the DRS, or the Au-TNTs should present higher degradation in the visible range, but this was not observed (see Fig. 4 and Figures S16 and S17). Gross et al., [18] evaluated the photoelectrochemical activity of modified TNTs with Ag nanoparticles, showing that the use of different radiations led to different effects. When visible light was used, the presence of Ag nanoparticles led to a positive effect probably related to the plasmon resonance effect, but under UV-Vis light, a negative effect was observed, related to a possible act of Ag as recombination center. Therefore, the behavior of silver is not always negative or positive and can be influenced by the type of radiation applied. Interestingly, in other work, Sun et al., [48] reported better performance for TNTs modified with Ag nanoparticles than bare TNTs under UVA illumination, and Xiao [49] showed that the photocatalytic degradation of methyl orange using the same type of radiation was favored for Ag- > Pt- > Au- > bare-TNTs. These studies suggest that for UVA or visible radiation the use of Ag nanoparticles can be beneficial, while for another type of UV radiation, the presence of this metal is not advantageous, as also shown in this work for UV-Vis radiation.

In literature, it is also shown that the role of each metal for the catalytic and photocatalytic activities is different. For example, Xiao [27] obtained the highest catalytic activity order of Au > Ag > Pt NPs with the bare TNTs presenting negligent catalytic reduction of nitrophenol toward 4-aminophenol, while the photocatalytic order was Pt- > Au- > Ag- > bare TNTs. When the nanotubes were obtained via a second anodization step, the metal dispersion was easier due to the obtention a smooth nanotubes surface [27,49]. This allowed to have a change in the catalytic performance to Au-/Ag- > Pt- > bare TNTs and the photocatalytic activity was Ag- > Pt- > Au- > bare TNTs [49]. Also, the analysis of these two studies allowed to understand that the catalytic activity is also dependent on the amount of the deposited metal and its dispersion, with the nanotubes surface smoothness being a parameter that affects the catalytic performance by influencing the metal dispersion [27,49].

To conclude, the increase in the metal loads can change the nanoparticle sizes and an excessive presence of the nanoparticles can cover the TiO_2 active sites hindering the performance of decorated TNTs [30].

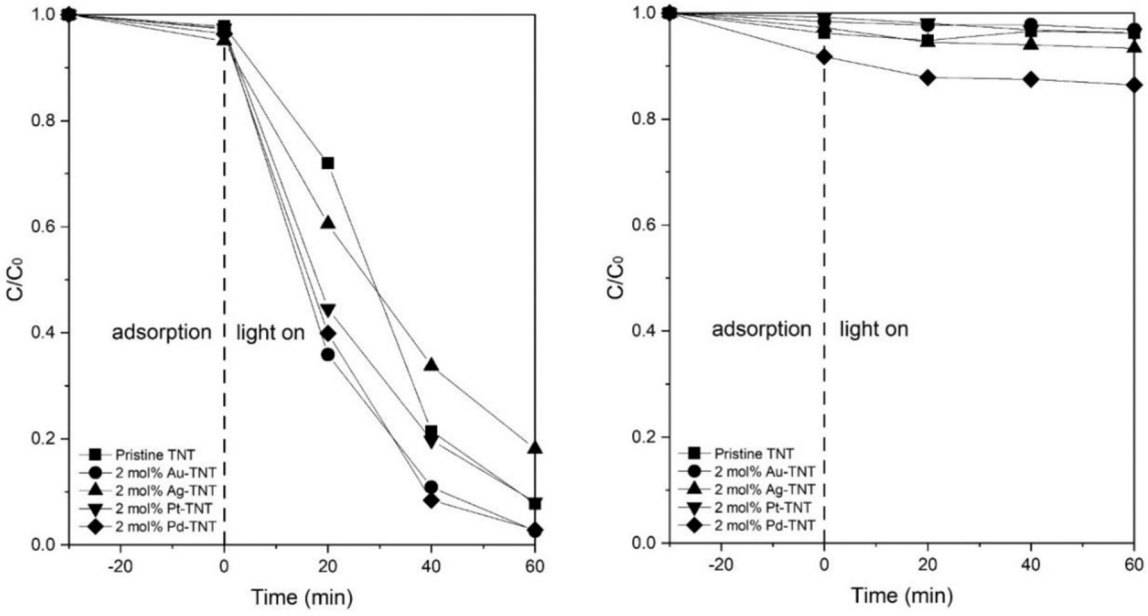

Fig. 7. Phenol photodegradation with Pristine and 2 mol% modified TNTs for UV-Vis (left) and Vis radiation (right).

Moreover, the metal loads can also influence the catalytic activity [27, 49]. Therefore, an evaluation of the synergetic effect between the load of metal and surface morphology should be carried out to obtain the best photocatalytic/catalytic activity. The noble metals may enhance the photocatalytic activity by acting as an electron receptor and decreasing the pairs recombination, providing additional surface area or by increasing the generation of electrons and injecting them in the conduction band of the semiconductor as described by the hot electron mechanism [11,50]. The visible light irradiation causes the transference of electrons to the TiO_2 due to the formation of a Schottky barrier in the metal/semiconductor interface, providing these electrons to the conduction band and causing the generation of superoxide anion radicals [11]. Also, the noble metal NPs can act as catalysts in ozonation as example, benefiting the decomposition of ozone into hydroxyl radicals [19]. The pristine TiO_2 is not activated with visible light, and therefore, the degradation is mainly related to absorption mechanisms. The type of radiation can also influence the effect of the metal presence (as discussed in the case of Ag). Moreover, different metals can present different behaviors and performances when are used in a photocatalytic or catalytic reaction.

3.3. By-products analysis

Reaction by-products are formed during the photocatalytic degradation of phenol. The reaction by-products can be more recalcitrant and toxic than the initial compounds, resulting in worse impacts than the ones caused by the initial solution, so it is important to understand the efficacy of the applied treatment and the impacts of the treated wastewater. Beltrán et al., [51] identified benzoquinone, polyphenols (resorcinol, hydroquinone, and 1,2 – dihydroxybenzene), unsaturated carboxylic acids (fumaric and maleic acids), and saturated carboxylic acids (glyoxylic, oxalic, and formic acids) as phenol intermediates in different oxidation processes. For photolysis and photocatalysis with TiO_2 using a full UV spectrum irradiation source, the authors only identified polyphenols, as in the present work. In this work, four different phenol by-products (benzoquinone, resorcinol, hydroquinone, and 1,2 – dihydroxybenzene) were identified in the treated water samples. Due to this complex task, detailed results about the by-product formation (under UV-Vis and Vis radiation) are presented in complementary information (Figure S18-S37). Regarding to this topic, the general results show that the by-products formation is dependent on the radiation, photocatalyst and amount of metal deposited in the TNTs during the photocatalytic reaction, which suggests different pathways and kinetic rates.

3.3.1. By-products analysis considering UV-Vis radiation

Considering the UV-Vis radiation, the use of pristine-TNTs favored the formation of 1,2 – dihydroxybenzene (catechol), followed by hydroquinone, benzoquinone, and resorcinol. For the 2 mol% samples, this formation is also favored in the case of Au, while for the Ag, hydroquinone reaches a higher concentration than the 1,2 – dihydroxybenzene at 20 min. For 2 mol% Pt-TNTs, resorcinol and benzoquinone present similar profiles with the resorcinol presenting higher concentration after 60 min. For the Pd-TNTs, benzoquinone presents higher concentration than hydroquinone at 20 min. Interestingly, different conclusions are taken when comparing to the 1 mol% samples, in which the present sequence is favored for the 1 mol% Au-, Pd- and Pt-TNTs, while the 1 mol% Ag-TNTs present hydroquinone with higher concentration at 20 min (Figure S30-S33). Moreover, other considerations can be seen. For example, in the case of benzoquinone, the use of 1 mol% of Pt- or Pd-TNTs led to the highest generation of this by-product, while the 1 mol% Au-TNT presented a negligible formation of the same by-product, only at 20 min. However, in the case of 1,2 – dihydroxybenzene, the Au sample leads to higher formation of this by-product when compared to the Pd and Pt samples (See Figure S25). Similar conclusions happen if hydroquinone is considered (see Figure S23).

These observations suggest that different degradation mechanisms and kinetics occurs in this system, and that is dependent on the sample (metal and amount) considered. One explanation for this can be related to a different generation (in terms of amount and type) of oxidizing species, that should be influenced by the selected photocatalyst. Noble metal clusters may favor the formation of superoxide anion radicals [52], which may affect the by-products generation. Moreover, metals may act as recombination centers depending on the metal amount [52]. This recombination was also noted to occur in transition metals as V, Mo, Cr, W, Fe, Co, and Cu as the metal load increased from 0.3 to 5 mol% [53]. In the work of Espino-Estévez et al., [34], also different formation and degradation rates for phenol, resorcinol, hydroquinone, and catechol occurred when powder TiO_2, Pd-TiO_2, and Ag-TiO_2 were used. Therefore, these considerations support the hypothesis of different

kinetics and degradation pathways caused by a different generation and role of oxidation radicals due to the different modified photocatalysts.

During this analysis, it is also possible to note another consideration. At 60 min, the by-product concentration is lower than at 20 min, which may suggest that the by-products start to be attacked after a low concentration of phenol. This can be a sign of the material's photoactivity since high photoactive materials should lead to higher degradation rates (of phenol and even generated by-products). Fig. 8 present the generation of the studied by-products during the phenol photodegradation under UV-Vis radiation.

The presence of hydroxyl radicals should favor the formation of 1,2 – dihydroxybenzene (catechol) and hydroquinone [54], and from Fig. 8, it is observed a higher concentration of catechol followed by hydroquinone, which suggests that the •OH should play an important role in the degradation mechanism of phenol for these conditions. Moreover, after hydroquinone, the other compound with higher concentration is benzoquinone, which can be obtained from hydroquinone due to the action of •OH radicals [51,55] (see also Figures S30-S33 from supporting information). Furthermore, resorcinol can be formed due to the action of holes [54].

In the case of photocatalytic oxidation (16 W UVC radiation) of a dye with Pt-TNTs, Hajjaji et al., [50] showed that the radicals responsible for the degradation of a dye was hole (h^+) > hydroxyl radical (•OH) > superoxide anion radical ($\bullet O_2^-$), with hole and hydroxyl radical showing a major role, while the superoxide having only a partial contribution in the degradation. In the photocatalysis mechanism, the electron (e^-) is promoted to the conduction band forming a hole (h^+) in the valence band, through the irradiation of TiO_2. After, the h^+ reacts with H_2O forming •OH, while the e^- reacts with the dissolved oxygen forming $\bullet O_2^-$. These radicals can react with the pollutants towards mineralization [9]. Even during this mechanism, hydroperoxyl radicals (•OOH) can be formed through the reaction between the $\bullet O_2^-$ and an H^+, and react with the pollutants or form H_2O_2, which can posteriorly also form •OH [9]. Analyzing this mechanism, the use of a hole (h^+) scavenger can stop the formation of •OH and •OOH radicals, and therefore the degradation only occurs by the action of $\bullet O_2^-$, which may have a poor contribution. When a •OH scavenger is used, it only inhibits this radical action, allowing •OOH and $\bullet O_2^-$ radicals to be formed and posteriorly react, with the •OOH radicals suggesting better action than the $\bullet O_2^-$ radicals in the work of Hajjaji et al., [50]. That is the reason why the h^+ has responsibility in the degradation of contaminants by photocatalysis. Interestingly, Abdelfattah and Ismail [56] studied the removal of phenol from real wastewater of a pharmaceutical industry using powder TiO_2 under UVA radiation, with the mechanistic studies showing a major contribution of •OH followed by $\bullet O_2^-$, while Seal and Chaudhuri [57] used TiO_2 and UVC radiation with the same conclusions being taken, which suggests that the type of target pollutant influences the contribution of radicals. Also, this contribution seems to not be affected by the type of UV radiation, although both works cannot be directly compared. Nevertheless, Lv et al., [54] suggested the formation of resorcinol due to the phenol oxidation via photogenerated holes, using TiO_2 P25 and UVA radiation.

Therefore in this case it is expected to have a major contribution of •OH followed by $\bullet O_2^-$ radical, which is concordant to the intermediate compounds formation mechanism, with the possiblity of existing also the participation of holes in the formation of resorcinol. Although the presence of metals may favor the formation of superoxide anion radical, it seems that the •OH has the major role in the phenol degradation mechanism, making it possible to see a certain effect in the by-products formation due to the presence and amount of different metals. Also, the type of radiation used in the experiments (UV-Vis) is capable of generating charge carriers from the TiO_2 [6] which explains the existence of

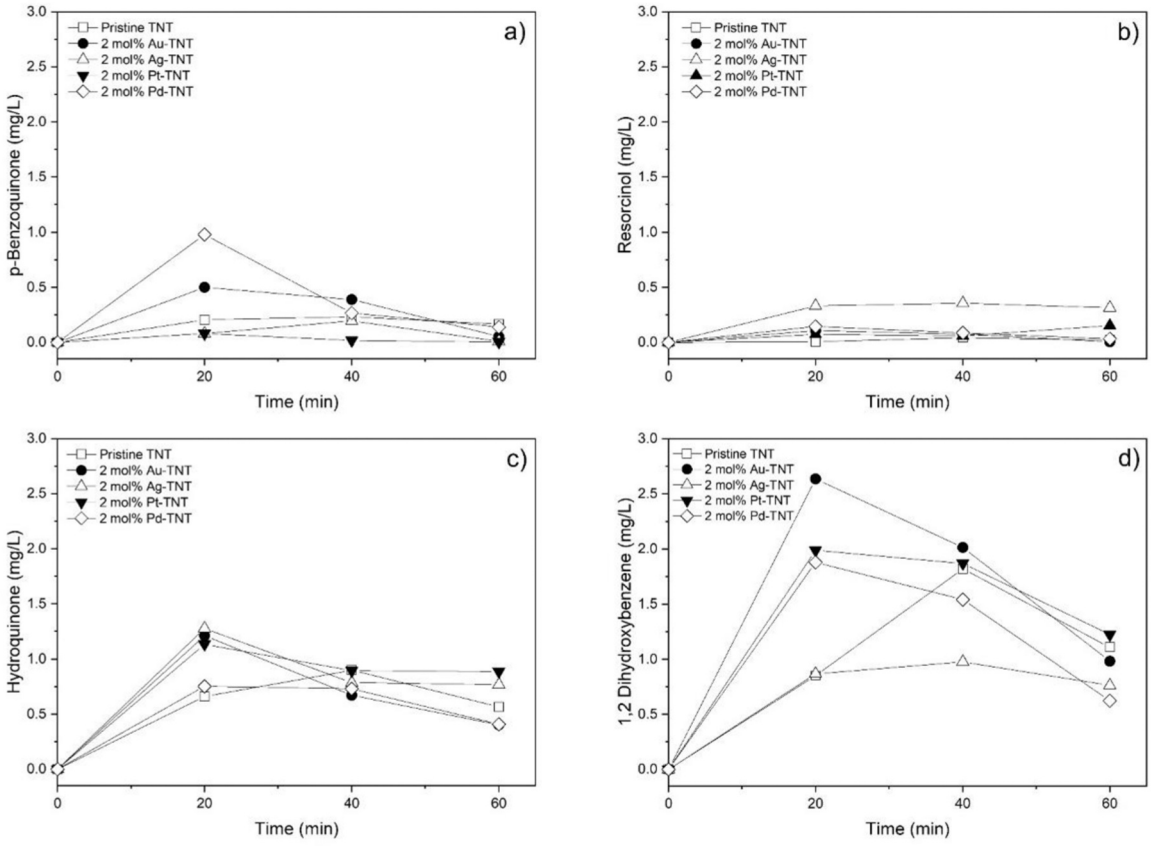

Fig. 8. By-products analysis of phenol photocatalytic oxidation with UV-Vis radiation: (a) p-benzoquinone, (b) resorcinol, (c) hydroquinone and (d) 1,2-dihydroxybenzene.

•OH radicals in the reaction. However, this consideration is only suggested considering the generated byproducts and a possible generation mechanism. No complementary studies involving different radicals scavengers were carried to attest or refuse this hyphotesis.

Regarding to the phenol degradation using a commercial TiO_2 particle under UVC radiation, Dang et al., [58] identified two main stages of phenol photodegradation, phase I which comprises the degradation of phenol to intermediate products, and the phase II comprises the mineralization of intermediate compounds to CO_2 and H_2O. This observation is concordant with the results obtained in this work, as mentioned. Analyzing the phenol degradation mechanism purposed in other works, other intermediate compounds (besides these selected four by-products) may be obtained such as pyrocatechol, 1,2,4-benzene-triol or carboxilic acids, such as maleic, salycylic, fumaric or oxalic acid [55, 58]. Other products such as hydroxyhydroquinone, hydroxybenzoquinone, butanol, acrolein, glycerol, acetylene dicarboxylate, salicyclic acid, muconic acid, or even others can be formed during phenol photodegradation [58].

3.3.2. *By-products analysis considering Vis radiation*

The material's behavior regarding the type/amount of by-product formation depends on the type of radiation applied in the photocatalytic process. The most evident difference is that from the four considered by-products, only benzoquinone was detected in very low amounts (see Fig. 9), although a non-identified intermediate compound was detected by HPLC. This poor formation and low concentration of by-products is related to the poor phenol degradation when visible radiation is considered. The visible radiation is not supposed to be capable of promoting the transference of an electron from the TiO_2 valence to the conduction band, which in turn does not start the traditional photocatalytic mechanism to form the •OH radicals. The modification of TNTs with noble metals has the objective of obtaining the plasmonic effect and get activity under visible light. This should allow the formation of superoxide anion radicals, and in turn, the phenol degradation. In their work, Zwara et al., [59] used $AgPO_3$ for the removal of phenol under visible radiation. The authors suggest that the degradation of phenol only occurs due to the LSPR effect of the Ag NPs, and that the electrons are transferred from the NPs to the $AgPO_3$ conduction band and trapped by the oxygen molecules adsorbed on the photocatalyst surface, forming the $\bullet O_2^-$ radicals. Then, these radicals react with phenol forming benzoquinone as the main by-product.

From Fig. 9, it is possible the formation of benzoquinone using pristine TNTs, which is not expected. Although the removal of phenol was only 3% in 60 min, this suggests the transformation of the phenol molecule. This transformation may occcur due to the pristine TNTs present some surface deffects in the crystallite structure, namely the existence of oxygen vacancies and Ti^{3+} in the TiO_2 crystallite structure [60]. This can happen during the annealing treatment, causing small visible light activity, and therefore, leading to some contaminant degradation. Other studies show degradation of contaminants under visible radiation for pristine TNTs [11,61] and powder TiO_2 [60].

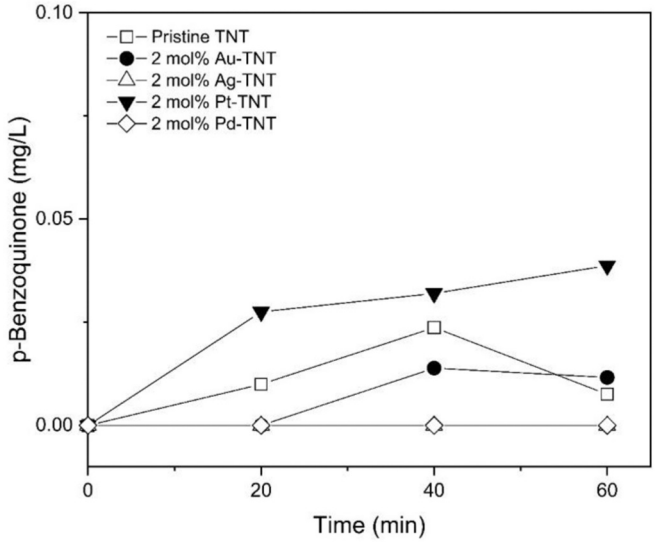

Fig. 9. By-products analysis of phenol photocatalytic oxidation with Vis radiation: p-benzoquinone.

In the case of UV-Vis radiation, it was seen that the preferential mechanism was for the formation of catechol, hydroquinone, benzoquinone, and resorcinol, respectively, but when visible radiation replaces the UV-Vis, benzoquinone is the preferential by-product to be formed (see Figures S34-S37). In this case, no signs of hydroquinone were found, so the benzoquinone molecule appear due to the action of $\bullet O_2^-$ radical with the phenol molecule, which is concordant with an enhancing in the formation of this type of radical due to presence of the metal, as occurred in the work of Zwara et al., [59]. It is important to note that the benzoquinone was detected in the reaction using the photocatalyst under analysis in Fig. 9, except the 2 mol% Pd-TNTs probably due to the high degradation observed. When the 2 mol% Ag-TNTs was used, this intermediate product was possible to be detected, but not quantified.

Therefore, it is reported in this work that the differences between the by-products formation mechanism and the concentrations are dependent on the photocatalysts, metal load, and irradiation source. Fig. 10 present a purposed mechanism for the studied by-products for UV-Vis and Vis radiation based on literature [54,55,59]. Nevertheless, when visible radiation is used, hydroquinone may also be formed in some cases due to the transformation of $\bullet O_2^-$ radicals into •OH radicals [62]. Under UVC radiation it is also possible to have the transformation in each other of catechol and benzoquinone due to electrons exchange. This occurs due to the molecules instability in a process called electrogenerated chemiluminescence [58].

3.4. *Evaluation of TNTs reuse*

Several studies report difficult recover and efficiency loss after reusing powder TiO_2 [63,64]. Due to the process economic viability, the photocatalyst reuse should be an important aspect to consider.

Costa and Prado [64] showed loss of 90% activity (after 9 uses) for anatase TiO_2 and difficulties in the powder recover, while TiO_2 nanotubes in powder only presented a loss of 10%. The loss of activity is related to loss of mass during the recovering operation, in which the TiO_2 nanotubes in powder revealed to be easier to separate. These losses will negatively influence the process by requiring specific separation and recover operations, but also "fresh" material will need to be added to balance the material loss. This can limit the economic feasibility and project implementation, since these drawbacks affect the operational costs, the investment capital, and the treatment plant design.

The TNTs can avoid these aspects since they are very robust and therefore be a suitable solution to implement [65]. However, TNTs can have loss of performance due to catalyst poisoning [20], so it is important to understand how many treatments cycles the TNTs present good performance can. The TNTs can also suffer from surface fouling [46]. To evaluate this topic, Fig. 11 present the pristine TNTs reuse performance in the phenol abatement.

The TNTs revealed to be stable after 7 reuses, with other reports presenting similar conclusions for 4 reuses [20]. Moreover, Gomes et al., [66] showed that TNTs maintained the morphological and crystallite properties after 15 uses in catalytic and photocatalytic ozonation, while Lincho et al., [19] reported that after at least 15 uses under UVA or Solar photocatalysis, catalytic, or photocatalytic ozonation, the TNTs performance was practically the same.

Therefore, these considerations suggests that the TNTs are versatile and stable for the use in different advanced oxidation processes,

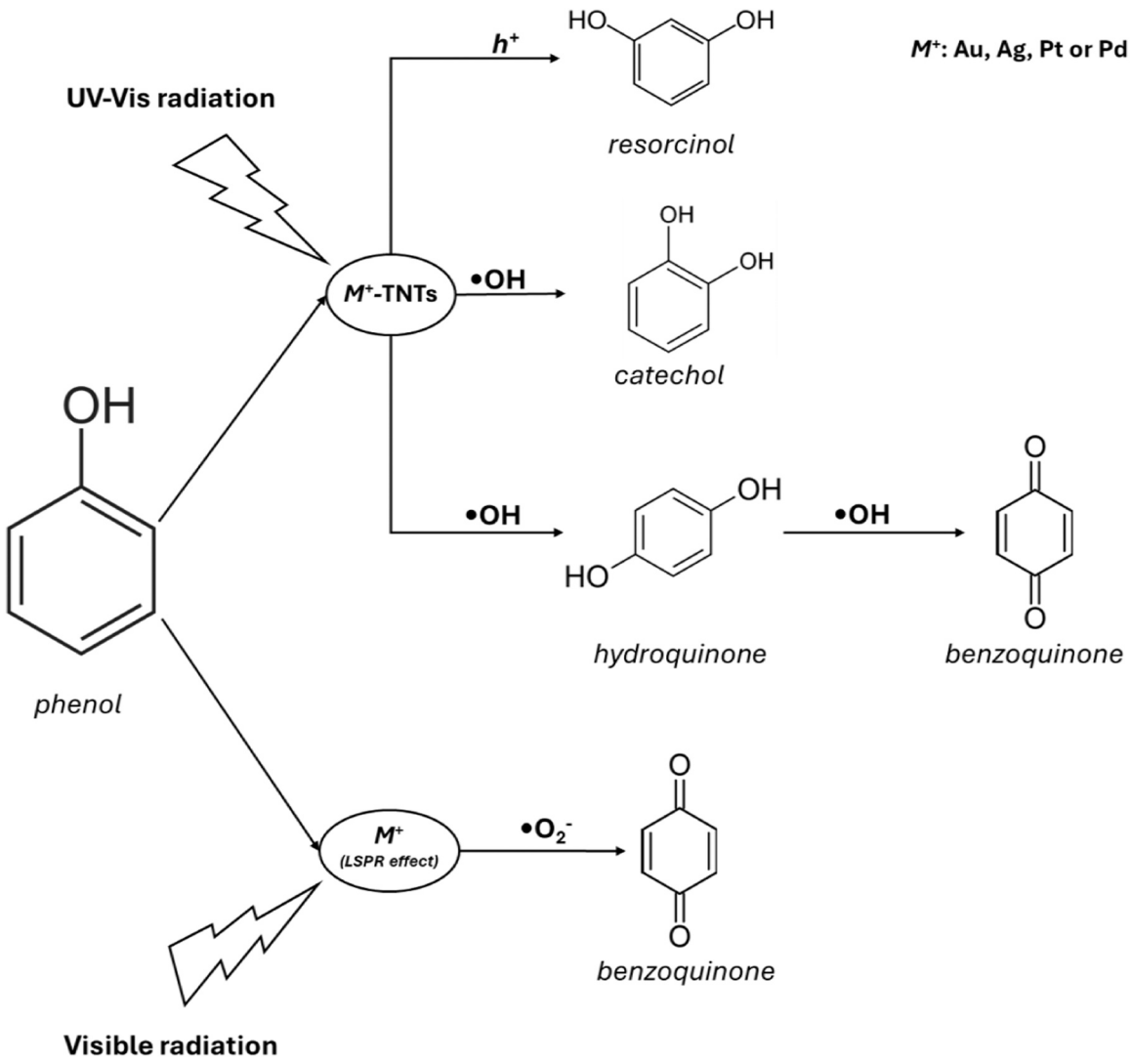

Fig. 10. Purposed mechanism for the generation of the studied by-products.

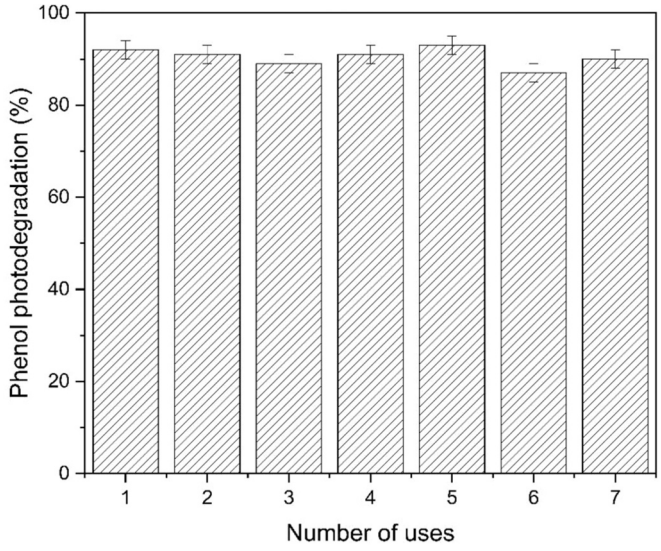

Fig. 11. Reuse of Pristine TNTs in the photodegradation of phenol with UV-Vis radiation.

overcoming one of the worse drawbacks of powder photocatalysts. Even in the case of suffering from surface poisoning, a simple thermal treatment (calcination conditions suggested) or a simple cleaning and storage for a few months should regenerate the catalyst activity [46,63]. In conclusion, comparing powder and anodized TNTs, it seems that the latter show more appealing features for the application at industrial level.

4. Conclusion

TiO_2 nanotubes were successfully obtained by the anodization method and modified by the photodeposition method, comprising the decoration with one of four different noble metals (Au, Ag, Pt and Pd) at different metal loads (0.5, 0.75, 1, 2 or 5 mol%). The TNTs can present a suitable option to obtain supported photocatalysts able to be separated from the liquid phase, recovered, and reused, overcoming one of the most important drawbacks pointed to the photocatalytic oxidation with TiO_2.

The SEM analysis indicated the presence of metals deposited in the nanotube top as well as a nanotube length of 4 μm. Due to the calcination parameters, all the samples showed the presence of the anatase phase with a bandgap energy of 3.1–3.2 eV. The decoration with metals decreased the recombination rate of photogenerated carriers for most of the samples, as confirmed by PL measurements.

Under UV-Vis radiation, pristine led to 92% phenol removal in 60 min, while the best degradation occurred for 2 and 5 mol% of Au-TNTs and 0.75, 1 and 2 mol% of Pd-TNTs which achieved 97% phenol removal. Ag- and Pt- metals did not significantly increase the phenol degradation or its rate, with the presence of Ag causing a disadvantage in this case. Under Vis radiation, the best samples were obtained with 1, 2 and 5 mol% Pd-TNTs with 12%, 14% and 13% phenol removal, respectively. With this radiation, Ag-, Pt- and Pd- metals presented a positive effect causing phenol degradation due to the LSPR effect. The Au-TNTs did not show advantages.

The by-products analysis considering four different products under UV-Vis radiation shows a preferential formation of catechol, hydroquinone, benzoquinone, and resorcinol respectively, which can be explained by a major contribution of •OH radicals. At low phenol concentration, the radicals start to attack the formed by-products. Under Vis radiation, benzoquinone was the only by-product formed at very low concentrations. This is concordant with the low phenol degradation as well as the formation and action of $\bullet O_2^-$ radical, which is generated due to the LSPR effect promoted by the metal presence. In general, the by-products analysis showed that different degradation mechanisms and kinetic rates occur when different metal types, metal loads or types of radiation are considered.

CRediT authorship contribution statement

João Lincho: Writing – original draft, Visualization, Methodology, Investigation, Data curation, Conceptualization. **Pawel Mazierski**: Writing – review & editing, Methodology, Investigation, Data curation, Conceptualization. **Tomasz Klimczuk**: Methodology, Investigation, Data curation. **Rui C. Martins**: Writing – review & editing, Supervision, Methodology, Conceptualization. **João Gomes**: Writing – review & editing, Supervision, Methodology, Conceptualization. **Adriana Zaleska-Medynska**: Writing – review & editing, Supervision, Methodology, Conceptualization.

Declaration of Competing Interest

The authors declare that they have no known competing financial interests or personal relationships that could have appeared to influence the work reported in this paper.

Data Availability

Data will be made available on request.

Acknowledgments

The authors gratefully acknowledge the Foundation for Science and Technology – FCT (Portugal) for the PhD grant (2021.06221.BD) with DOI 10.54499/2021.06221.BD (https://doi.org/10.54499/2021.06221.BD). The author J.G. gratefully acknowledges FCT (Portugal) by the financial support (CEECIND/01207/2018).

Appendix A. Supporting information

Supplementary data associated with this article can be found in the online version at doi:10.1016/j.jece.2024.112990.

References

[1] J.M. Macak, H. Tsuchiya, A. Ghicov, K. Yasuda, R. Hahn, S. Bauer, P. Schmuki, TiO2 nanotubes: self-organized electrochemical formation, properties and applications, Curr. Opin. Solid State Mater. Sci. *11* (1–2) (2007) 3–18.
[2] V. Galstyan, J.M. Macak, T. Djenizian, Anodic TiO2 nanotubes: a promising material for energy conversion and storage, Appl. Mater. Today *29* (2022) 101613.
[3] O. Carp, C.L. Huisman, A. Reller, Photoinduced reactivity of titanium dioxide, Prog. Solid State Chem. 145 (2004).
[4] A.Y. Shan, T.I. Mohd Ghazi, S.A. Rashid, Immobilisation of titanium dioxide onto supporting materials in heterogeneous photocatalysis: a review, Appl. Catal. A-Gen. *389* (1–2) (2010) 1–8.
[5] M. Zlamal, J. Macak, P. Schmuki, J. Krysa, Electrochemically assisted photocatalysis on self-organized TiO2 nanotubes, Electrochem. Commun. *9* (12) (2007) 2822–2826.
[6] P. Mazierski, M. Nischk, M. Gołkowska, W. Lisowski, M. Gazda, M.J. Winiarski, T. Klimczuk, A. Zaleska-Medynska, Photocatalytic activity of nitrogen doped TiO2 nanotubes prepared by anodic oxidation: the effect of applied voltage, anodization time and amount of nitrogen dopant, Appl. Catal. B. *196* (2016) 77–88.
[7] H. Sopha, Y. Norikawa, M. Motola, L. Hromadko, J. Rodriguez-Pereira, J. Cerny, T. Nohira, K. Yasuda, J.M. Macak, Anodization of electrodeposited titanium films towards TiO2 nanotube layers, Electrochem. Commun. *118* (2020) 106788.
[8] H. Sopha, M. Baudys, M. Krbal, R. Zazpe, J. Prikryl, J. Krysa, J.M. Macak, Scaling up anodic TiO2 nanotube layers for gas phase photocatalysis, Electrochem. Commun. *97* (2018) 91–95.
[9] M. Pelaez, N.T. Nolan, S.C. Pillai, M.K. Seery, P. Falaras, A.G. Kontos, P.S. M. Dunlop, J.W.J. Hamilton, J.A. Byrne, K. O'Shea, M.H. Entezari, D.D. Dionysiou, A review on the visible light active titanium dioxide photocatalysts for environmental applications, Appl. Catal. B. *125* (2012) 331–349.
[10] F. Riboni, L.G. Bettini, D.W. Bahnemann, E. Selli, WO3–TiO2 vs. TiO2 photocatalysts: Effect of the W precursor and amount on the photocatalytic activity of mixed oxides, Catal. Today *209* (2013) 28–34.
[11] A. Merenda, M. Weber, M. Bechelany, F.-M. Allioux, L. Hyde, L. Kong, L.F. Dumée, Fabrication of Pd-TiO2 nanotube photoactive junctions via atomic layer deposition for persistent pesticide pollutants degradation, Appl. Surf. Sci. *483* (2019) 219–230.
[12] H. Yu, X. Wang, H. Sun, M. Huo, Photocatalytic degradation of malathion in aqueous solution using an Au–Pd–TiO2 nanotube film, J. Hazard. Mater. *184* (1–3) (2010) 753–758.
[13] J. Huang, L. Ding, Y. Xi, L. Shi, G. Su, R. Gao, W. Wang, B. Dong, L. Cao, Efficient silver modification of TiO 2 nanotubes with enhanced photocatalytic activity, Solid State Sci. *80* (2018) 116–122.
[14] J. Lv, H. Gao, H. Wang, X. Lu, G. Xu, D. Wang, Z. Chen, X. Zhang, Z. Zheng, Y. Wu, Controlled deposition and enhanced visible light photocatalytic performance of Pt-modified TiO2 nanotube arrays, Appl. Surf. Sci. *351* (2015) 225–231.
[15] S. Bai, J. Jiang, Q. Zhang, Y. Xiong, Steering charge kinetics in photocatalysis: intersection of materials syntheses, characterization techniques and theoretical simulations, Chem. Soc. Rev. *44* (10) (2015) 2893–2939.
[16] M. Rycenga, C.M. Cobley, J. Zeng, W. Li, C.H. Moran, Q. Zhang, D. Qin, Y. Xia, Controlling the synthesis and assembly of silver nanostructures for plasmonic applications, Chem. Rev. *111* (6) (2011) 3669–3712.
[17] H. Li, X. Duan, G. Liu, X. Liu, Photochemical synthesis and characterization of Ag/TiO2 nanotube composites, J. Mater. Sci. *43* (5) (2008) 1669–1676.
[18] P.A. Gross, S.N. Pronkin, T. Cottineau, N. Keller, V. Keller, E.R. Savinova, Effect of deposition of Ag nanoparticles on photoelectrocatalytic activity of vertically aligned TiO2 nanotubes, Catal. Today *189* (1) (2012) 93–100.
[19] J. Lincho, E. Domingues, P. Mazierski, M. Miodyńska, T. Klimczuk, A. Zaleska-Medynska, R.C. Martins, J. Gomes, The role of noble metals in TiO2 nanotubes for the abatement of parabens by photocatalysis, catalytic and photocatalytic ozonation, Sep. Purif. Technol. *326* (2023) 124747.
[20] M. Nischk, P. Mazierski, M. Gazda, A. Zaleska, Ordered TiO2 nanotubes: the effect of preparation parameters on the photocatalytic activity in air purification process, Appl. Catal. B. *144* (2014) 674–685.
[21] D. Regonini, C.R. Bowen, A. Jaroenworaluck, R. Stevens, A review of growth mechanism, structure and crystallinity of anodized TiO2 nanotubes, Mater. Sci. Eng. R. Rep. *74* (12) (2013) 377–406.
[22] J. Lincho, A. Zaleska-Medynska, R.C. Martins, J. Gomes, Nanostructured photocatalysts for the abatement of contaminants by photocatalysis and photocatalytic ozonation: an overview, Sci. Total Environ. *837* (2022) 155776.
[23] H. Xu, Q. Zhang, C. Zheng, W. Yan, W. Chu, Application of ultrasonic wave to clean the surface of the TiO2 nanotubes prepared by the electrochemical anodization, Appl. Surf. Sci. *257* (20) (2011) 8478–8480.
[24] J.M. Macak, H. Hildebrand, U. Marten-Jahns, P. Schmuki, Mechanistic aspects and growth of large diameter self-organized TiO2 nanotubes, J. Electroanal. Chem. *621* (2) (2008) 254–266.
[25] A. Valota, D.J. LeClere, P. Skeldon, M. Curioni, T. Hashimoto, S. Berger, J. Kunze, P. Schmuki, G.E. Thompson, Influence of water content on nanotubular anodic titania formed in fluoride/glycerol electrolytes, Electrochim. Acta *54* (18) (2009) 4321–4327.
[26] J. Yoo, R. Zazpe, G. Cha, J. Prikryl, I. Hwang, J.M. Macak, P. Schmuki, Uniform ALD deposition of Pt nanoparticles within 1D anodic TiO2 nanotubes for photocatalytic H2 generation, Electrochem. Commun. *86* (2018) 6–11.
[27] F. Xiao, An efficient layer-by-layer self-assembly of metal-TiO2 nanoring/nanotube heterostructures, M/T-NRNT (M = Au, Ag, Pt), for versatile catalytic applications, Chem. Commun. *48* (52) (2012) 6538.
[28] V.C. Anitha, R. Zazpe, M. Krbal, J. Yoo, H. Sopha, J. Prikryl, G. Cha, S. Slang, P. Schmuki, J.M. Macak, Anodic TiO2 nanotubes decorated by Pt nanoparticles using ALD: an efficient electrocatalyst for methanol oxidation, J. Catal. *365* (2018) 86–93.
[29] L. Assaud, N. Brazeau, M.K.S. Barr, M. Hanbücken, S. Ntais, E.A. Baranova, L. Santinacci, Atomic layer deposition of Pd nanoparticles on TiO_2 nanotubes for ethanol electrooxidation: synthesis and electrochemical properties, ACS Appl. Mater. Interfaces *7* (44) (2015) 24533–24542.

[30] S.K. Mohapatra, N. Kondamudi, S. Banerjee, M. Misra, Functionalization of self-organized TiO_2 nanotubes with Pd nanoparticles for photocatalytic decomposition of dyes under solar light illumination, Langmuir *24* (19) (2008) 11276–11281.
[31] O.K. Varghese, D. Gong, M. Paulose, C.A. Grimes, E.C. Dickey, Crystallization and high-temperature structural stability of titanium oxide nanotube arrays, J. Mater. Res. *18* (1) (2003) 156–165.
[32] J. Zhang, P. Zhou, J. Liu, J. Yu, New understanding of the difference of photocatalytic activity among anatase, rutile and brookite TiO_2, Phys. Chem. Chem. Phys. *16* (38) (2014) 20382–20386.
[33] W.F. Zhang, Y.L. He, M.S. Zhang, Z. Yin, Q. Chen, Raman scattering study on anatase TiO_2 nanocrystals, J. Phys. D: Appl. Phys. *33* (8) (2000) 912–916.
[34] M.R. Espino-Estévez, C. Fernández-Rodríguez, O.M. González-Díaz, J. Araña, J. P. Espinós, J.A. Ortega-Méndez, J.M. Doña-Rodríguez, Effect of TiO2–Pd and TiO2–Ag on the photocatalytic oxidation of diclofenac, isoproturon and phenol, Chem. Eng. J. *298* (2016) 82–95.
[35] S.T. Nishanthi, S. Iyyapushpam, B. Sundarakannan, E. Subramanian, D. Pathinettam Padiyan, Significance of crystallinity on the photoelectrochemical and photocatalytic activity of TiO2 nanotube arrays, Appl. Surf. Sci. *313* (2014) 449–454.
[36] Y.K. Lai, L. Sun, C. Chen, C.G. Nie, J. Zuo, C.J. Lin, Optical and electrical characterization of TiO2 nanotube arrays on titanium substrate, Appl. Surf. Sci. *252* (4) (2005) 1101–1106.
[37] P. Mazierski, J. Nadolna, W. Lisowski, M.J. Winiarski, M. Gazda, M. Nischk, T. Klimczuk, A. Zaleska-Medynska, Effect of irradiation intensity and initial pollutant concentration on gas phase photocatalytic activity of TiO2 nanotube arrays, Catal. Today *284* (2017) 19–26.
[38] S. Lal, S. Link, N.J. Halas, Nano-optics from sensing to waveguiding, Nat. Photonics 1 (2007) 641–648.
[39] H.B. Jeon, P.V. Tsalu, J.W. Ha, Shape effect on the refractive index sensitivity at localized surface plasmon resonance inflection points of single gold nanocubes with vertices, Sci. Rep. 9 (2019) 13635.
[40] Z. Wu, Z. Sheng, Y. Liu, H. Wang, N. Tang, J. Wang, Characterization and activity of Pd-modified TiO2 catalysts for photocatalytic oxidation of NO in gas phase, J. Hazard. Mater. *164* (2–3) (2009) 542–548.
[41] X. Hu, Y. Shi, B. Zhu, S. Zhang, W. Huang, Highly photostable palladium-loaded TiO2 nanotubes and the active species in the photodegradation of methyl orange, Chin. J. Catal. *36* (2) (2015) 221–228.
[42] J. Gomes, J. Lincho, E. Domingues, M. Gmurek, P. Mazierski, A. Zaleska-Medynska, T. Klimczuk, R.M. Quinta-Ferreira, R.C. Martins, TiO2 nanotube arrays-based reactor for photocatalytic oxidation of parabens mixtures in ultrapure water: effects of photocatalyst properties, operational parameters and light source, Sci. Total Environ. *689* (2019) 79–89.
[43] F.J. Knorr, C.C. Mercado, J.L. McHale, Trap-state distributions and carrier transport in pure and mixed-phase TiO_2: influence of contacting solvent and interphasial electron transfer, J. Phys. Chem. C. *112* (33) (2008) 12786–12794.
[44] M. Klein, J. Nadolna, A. Gołąbiewska, P. Mazierski, T. Klimczuk, H. Remita, A. Zaleska-Medynska, The effect of metal cluster deposition route on structure and photocatalytic activity of mono- and bimetallic nanoparticles supported on TiO2 by radiolytic method, Appl. Surf. Sci. *378* (2016) 37–48.
[45] J. Reszczyńska, T. Grzyb, J.W. Sobczak, W. Lisowski, M. Gazda, B. Ohtani, A. Zaleska, Visible light activity of rare earth metal doped (Er3+, Yb3+ or Er3+/Yb3+) titania photocatalysts, Appl. Catal. B. *163* (2015) 40–49.
[46] S. Abela, C. Farrugia, R. Xuereb, F. Lia, E. Zammit, A. Rizzo, P. Refalo, M. Grech, Photocatalytic activity of titanium dioxide nanotubes following long-term aging, Nanomater 11 (2021) 2823.
[47] C. Farrugia, A. Di Mauro, F. Lia, E. Zammit, A. Rizzo, V. Privitera, G. Impellizzeri, M.A. Buccheri, G. Rappazzo, M. Grech, P. Refalo, S. Abela, Suitability of different titanium dioxide nanotube morphologies for photocatalytic water treatment, Nanomater 11 (2021) 708.
[48] L. Sun, J. Li, C. Wang, S. Li, Y. Lai, H. Chen, C. Lin, Ultrasound aided photochemical synthesis of Ag loaded TiO2 nanotube arrays to enhance photocatalytic activity, J. Hazard. Mater. *171* (1–3) (2009) 1045–1050.
[49] F. Xiao, Layer-by-layer self-assembly construction of highly ordered metal-TiO_2 nanotube arrays heterostructures (M/TNTs, M = Au, Ag, Pt) with tunable catalytic activities, J. Phys. Chem. C. *116* (31) (2012) 16487–16498.
[50] M.A. Hajjaji, K. Missaoui, K. Trabelsi, A. Bouzaza, B. Bessais, A. Hajjaji, A. A. Assadi, Electrodeposited platinum nanoparticles on highly ordered titanium dioxide nanotubes for photocatalytic application: enhancement of photocatalytic degradation of amido black dye, Catal. Lett. (2023).
[51] F.J. Beltrán, F.J. Rivas, O. Gimeno, Comparison between photocatalytic ozonation and other oxidation processes for the removal of phenols from water, J. Chem. Technol. Biotechnol. *80* (9) (2005) 973–984.
[52] P. Chowdhury, J. Moreira, H. Gomaa, A.K. Ray, Visible-solar-light-driven photocatalytic degradation of phenol with dye-sensitized TiO_2: parametric and kinetic study, Ind. Eng. Chem. Res. *51* (12) (2012) 4523–4532.
[53] S. Ikeda, N. Sugiyama, B. Pal, G. Marcí, L. Palmisano, H. Noguchi, K. Uosaki, B. Ohtani, Photocatalytic activity of transition-metal-loaded titanium(IV) oxide powders suspended in aqueous solutions: correlation with electron–hole recombination kinetics, Phys. Chem. Chem. Phys. *3* (2) (2001) 267–273.
[54] K. Lv, X. Guo, X. Wu, Q. Li, W. Ho, M. Li, H. Ye, D. Du, Photocatalytic selective oxidation of phenol to produce dihydroxybenzenes in a TiO2 /UV system: hydroxyl radical versus hole, Appl. Catal. B. *199* (2016) 405–411.
[55] L. Jothinathan, Q.Q. Cai, S.L. Ong, J.Y. Hu, Fe-Mn doped powdered activated carbon pellet as ozone catalyst for cost-effective phenolic wastewater treatment: mechanism studies and phenol by-products elimination, J. Hazard. Mater. *424* (2022) 127483.
[56] I. Abdelfattah, A.A. Ismail, Reduction of COD concentration and complete removal of phenol in industrial wastewater utilizing mesoporous TiO2 nanoparticles under UVA illumination, Opt. Mater. *145* (2023) 114410.
[57] K. Seal, H. Chaudhuri, A novel understanding of morphological anisotropy features of nanorod units in brookite dominated triphase mesoporous TiO2 and its excellent photocatalytic activity in phenol decomposition: the role of synthesis pH and surface hydroxylation, Surf. Interfaces *29* (2022) 101715.
[58] T.T.T. Dang, S.T.T. Le, D. Channei, W. Khanitchaidecha, A. Nakaruk, Photodegradation mechanisms of phenol in the photocatalytic process, Res. Chem. Intermed. *42* (6) (2016) 5961–5974.
[59] J. Zwara, E. Grabowska, T. Klimczuk, W. Lisowski, A. Zaleska-Medynska, Shape-dependent enhanced photocatalytic effect under visible light of Ag3PO4 particles, J. Photochem. Photobiol. A 367 (2018) 240–252.
[60] X. Bi, G. Du, A. Kalam, D. Sun, Y. Yu, Q. Su, B. Xu, A.G. Al-Sehemi, Tuning oxygen vacancy content in TiO_2 nanoparticles to enhance the photocatalytic performance, Chem. Eng. Sci. 234 (2021) 116440.
[61] N.K. Shrestha, M. Yang, Y.-C. Nah, I. Paramasivam, P. Schmuki, Self-organized TiO2 nanotubes: Visible light activation by Ni oxide nanoparticle decoration, Electrochem. Commun. *12* (2) (2010) 254–257.
[62] P. Mazierski, J. Łuczak, W. Lisowski, M.J. Winiarski, T. Klimczuk, A. Zaleska-Medynska, The ILs-assisted electrochemical synthesis of TiO2 nanotubes: The effect of ionic liquids on morphology and photoactivity, Appl. Catal. B 214 (2017) 100–113.
[63] S. Adhikari, K.S. Chandra, D.-H. Kim, G. Madras, D. Sarkar, Understanding the morphological effects of WO3 photocatalysts for the degradation of organic pollutants, Adv. Powder Technol. 29 (2018) 1591–1600.
[64] L.L. Costa, A.G.S. Prado, TiO2 nanotubes as recyclable catalyst for efficient photocatalytic degradation of indigo carmine dye, J. Photochem. Photobiol. A 201 (2009) 45–49.
[65] C. Farrugia, F. Lia, E. Zammit, A. Rizzo, V. Privitera, G. Impellizzeri, A. Di Mauro, M.A. Buccheri, G. Rapazzo, M. Grech, P. Refalo, S. Abela, Aging of anodic titanium dioxide nanotubes in synthetic greywater: assessment of stability and retention of photocatalytic activity, Mater. Chem. Phys. 272 (2021) 124986.
[66] J. Gomes, J. Lincho, P. Mazierski, M. Miodyńska, A. Zaleska-Medynska, R. C. Martins, Unexpected effect of ozone on the paraben's mixture degradation using TiO2 supported nanotubes, Sci. Total Environ. *743* (2020) 140831.